

Simulations of Axisymmetric Inertial Waves in a Rotating Container of Fluid

R. Batchelor¹, H.M. Blackburn¹ and R. Manasseh²

¹Department of Mechanical and Aerospace Engineering
 Monash University, Vic 3800, Australia

²Department of Mechanical Engineering
 Swinburne University, Vic 3122, Australia

Abstract

Coriolis accelerations in a rotating body of fluid produce restoring forces for disturbances that depart from solid-body rotation, resulting in wave-like motion known as inertial waves. This kind of behaviour can be important in geophysical and technological applications (e.g. planetary core dynamics, instabilities in spinning rocket fuel tanks). For simple container shapes and for solid-body rotations, the frequencies and mode shapes of inertia waves can be readily calculated following the assumptions of linearity and potential flow.

Our simulations seek to recreate the classic experiments of Fultz (1959) in which inertial waves within a cylindrical container of spinning fluid were driven via an axially oscillating disk situated on the container axis. Fultz found that the mode shapes and frequencies observed matched the linear inviscid predictions well, although it was unclear how exact resonance was assessed. We have employed a spectral element DNS method to carry out axisymmetric simulations with dimensionless parameters chosen to match those of Fultz's experiment, with varying cylinder geometries, and where the paddle motion was simulated by a fixed boundary within the fluid on which oscillatory boundary conditions were imposed. Resonance is assessed on the basis of maxima in the peak amount of flow kinetic energy for fixed paddle motion amplitude, or alternatively on the basis of minimum peak-to-peak force exerted on the paddle boundary. In general the mode shapes and resonance frequencies agree well with both the inviscid theoretical predictions and Fultz's published results.

Introduction

The motion of incompressible fluid taken relative to a frame of reference rotating about the z axis with angular velocity $\boldsymbol{\Omega} = \Omega \mathbf{k}$ is described by

$$\delta_t \mathbf{u} + \mathbf{u} \cdot \nabla \mathbf{u} + 2\boldsymbol{\Omega} \times \mathbf{u} = -\nabla p + \nu \nabla^2 \mathbf{u}, \quad \nabla \cdot \mathbf{u} = 0, \quad (1)$$

where $2\boldsymbol{\Omega} \times \mathbf{u}$ is the Coriolis acceleration and the kinematic pressure p includes a contribution from centripetal acceleration. We consider flow in a cylindrical container with height:radius ratio $H/R = \delta$ that rotates steadily about its axis. Considering disturbances to solid-body rotation flow in such a vessel, Coriolis acceleration provides a restoring force that tends to return a particle of fluid displaced from an initially circular streamline, resulting in inertial waves. If viscosity is neglected, the linearized Euler equations for an axisymmetric disturbance flow $\mathbf{u}(r, \theta, z)$ satisfy an eigenproblem which has a set of solutions described by [1]

$$u_r = -\kappa A J_1(\gamma_i r) \cos(n\pi z) \sin(\kappa t), \quad (2a)$$

$$u_\theta = \kappa A J_1(\gamma_i r) \cos(n\pi z) \cos(\kappa t), \quad (2b)$$

$$u_z = \kappa A \frac{\delta \gamma_i}{n\pi} J_0(\gamma_i r) \cos(n\pi z) \sin(\kappa t), \quad (2c)$$

where $\kappa = \kappa' / \Omega$, in which κ' is the angular frequency of oscillation and κ is a dimensionless frequency, A is an arbitrary amplitude, J_0, J_1 are Bessel functions of the first kind, γ_i are the i th zeros of J_1 (e.g. $\gamma_1 = 3.832, \gamma_2 = 7.016, \gamma_3 = 10.174$), n is a positive integer. Here lengths are nondimensionalised by the outer radius of the container, R , and times are nondimensionalised using the rotational speed Ω . The dimensionless period ratios for these eigenmodes is given by

$$\tau = \frac{\Omega}{\kappa'} = \frac{1}{2} \left[\left(\frac{\gamma_i}{n\pi} \right)^2 \delta^2 + 1 \right]^{\frac{1}{2}} \quad (3)$$

as shown in *Figure 1*. For each pair $i-n$ there is a separate solution, and as follows from eqns (1), each pair corresponds to a flow with i cells in the radial direction and n cells in the axial direction. Valid solutions exist only when $\tau \geq 0.5$, for which the set of Euler equations in the rotating frame is hyperbolic.

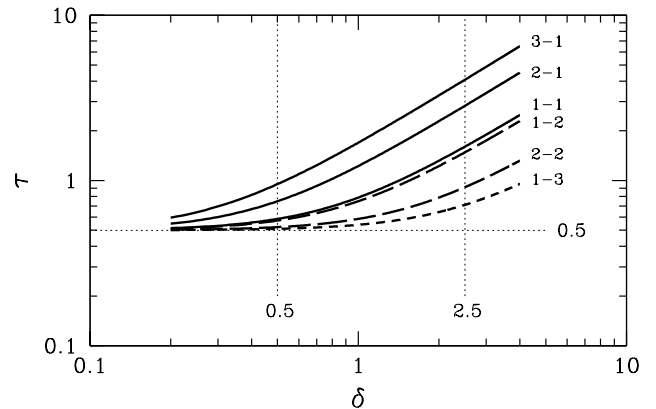


Figure 1. Dimensionless period ratios τ for Euler eigenmodes of oscillatory disturbances to solid-body rotation of flow in a cylindrical container of height:radius ratio δ , from eqn (3). Indices $i-n$ correspond to the number of circulation cells in the radial and axial directions respectively. Our simulations were carried out for $\delta = 0.5$ and 2.5 .

Fultz (1959) sought to investigate the system using an experiment in which the flow in a rotating tank was driven axially at frequency ω by an oscillating (and non-rotating) disk paddle with relative diameter 0.226. The set-up is illustrated in *Figure 2*: as can be seen in the flow visualisation photograph, in an experiment seeded with rheoscopic flakes, distinct linear features may be observed, corresponding to hyperbolic characteristics of the solution. Our focus here will be on aspects of resonance and cellular structure in simulations chosen to match Fultz's experiment but we note that our simulations will vary in some aspects: in the experiments, the upper surface of water in the tank

was open to atmosphere, whereas in our simulations, solid walls will enclose the flow on all sides. Also, we used a paddle that rotated with the tank, rather than one which did not. These differences do not seem to have been significant. Fultz assessed resonance (frequency matching) somewhat subjectively from observations of the motion of dye injected down the axis of the tube holding the paddle. The Reynolds number achieved in Fultz’s experiment was $Re = \Omega R^2/\nu = 6133$.

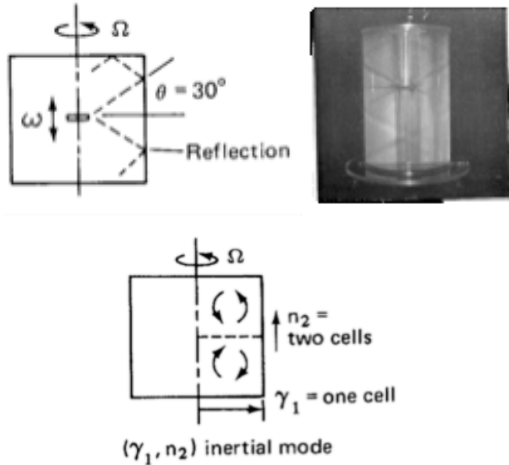


Figure 2. Schematic and flow visualization of rotating tank driven by an oscillating paddle, corresponding to Fultz’s (1959) experiment [1][2][3].

Numerical Method

The method we have used mimics Fultz’s experimental setup. We simulate the incompressible Navier–Stokes equations for axisymmetric flow with three velocity components using a spectral element algorithm developed for cylindrical coordinates [4]. Attention is restricted principally to two geometries, one with $\delta = 0.5$ and the other with $\delta = 2.5$. For the former, a mesh with 500 spectral elements was used while for the latter, 400 elements were employed. Semi-plane meshes for the case $\delta = 0.5$ are shown in Figure 3. For all simulations, nodal element shape functions with tensor products of polynomials of order $N = 6$ were employed.

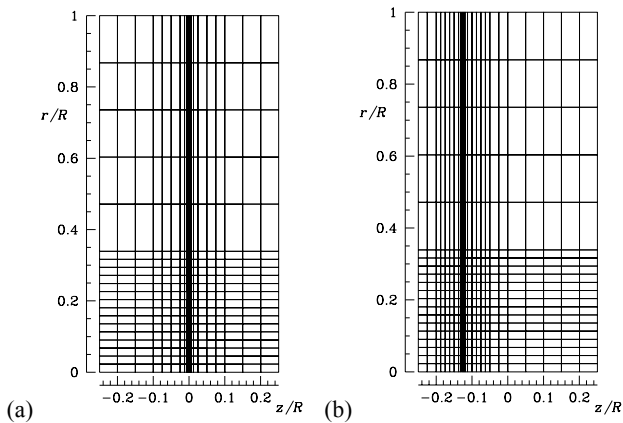


Figure 3. Spectral element semi-plane meshes for $\delta = 0.5$. Geometry adopted for modes with (a) n odd (i.e. odd numbers of axial cells) and (b) n even (even numbers of axial cells). In each case, the region where paddle-type boundary conditions were adopted (see text) is shown as a thick black line of extent $r/R=0.226$.

No-slip solid walls are used for all outer boundaries except at the axis, which is free-slip (zero Neumann) for axial velocity component and zero Dirichlet for radial and azimuthal components. The paddle was represented as a no-slip boundary, whose location was fixed but where the axial velocity is simple harmonic of prescribed frequency and amplitude. The paddle

location was varied depending on whether the axial mode index n of the mode of interest was odd, in which case the paddle was located at $z/H = 0$, or even, in which case the paddle was located at $z/H = -0.25$, as shown in Figure 3 (a) and (b), respectively. This allows the paddle to be placed near an axial antinode of the flow, and follows the methodology adopted by Fultz.

The flow was solved in the laboratory frame, i.e. with the tank and paddle walls moving steadily in the azimuthal direction with local magnitude $r\Omega$. This means that the Coriolis and centripetal acceleration terms were not explicitly represented. Flows were initiated with solid-body rotation and evolved until velocities recorded at a number of sampling points throughout the container reached limit-cycle states – this typically took of order 50 paddle motion cycles to achieve. For $\delta = 0.5$, Reynolds number $Re = 6133$, matching the value used in experiments, while for $\delta = 2.5$, the Reynolds number was reduced to $Re = 2154$.

Mode Shapes

Before turning to examine assessment of resonance we present in this section examples of mode shapes. In each plot, colour contours of instantaneous radial velocity component are shown overlaid with instantaneous streamlines. Cellular mode shapes are indicated by closed streamline cells, with the approximate position of the paddle tip marked by extremes of radial velocity.

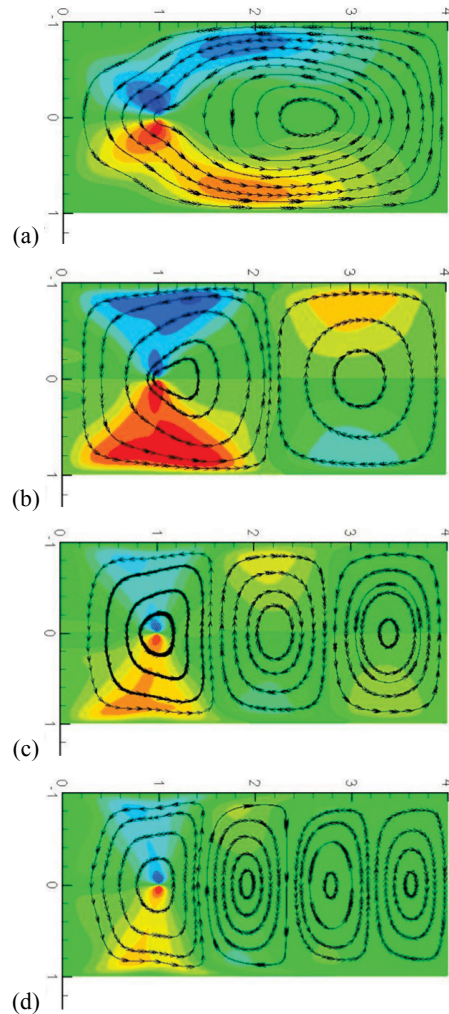


Figure 4. Example mode shapes for container geometry $\delta = 0.5$. Colour contours of radial velocity component overlaid with instantaneous sectional streamlines. All the cases shown have one axial cell ($n = 1$) and correspond to modes of $i-n$ indices (a) 1–1, with $\tau = 0.586$; (b) 2–1, $\tau = 0.749$; (c) 3–1, $\tau = 0.952$; (d) 4–1, $\tau = 1.173$.

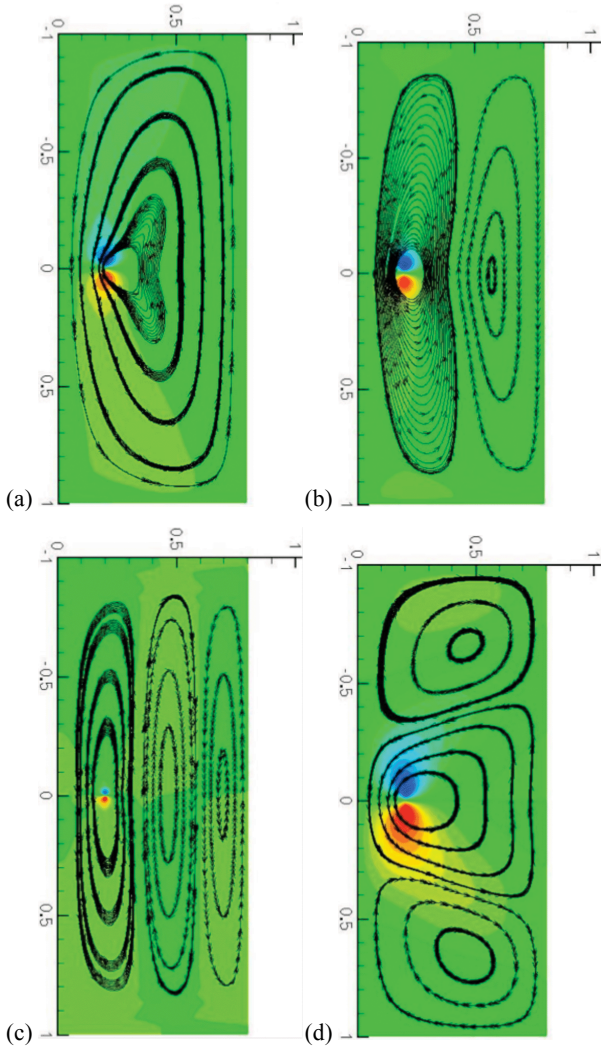


Figure 5. Example mode shapes for container geometry $\delta = 2.5$. Colour contours of radial velocity component overlaid with instantaneous sectional streamlines. Cases correspond to modes of i - n indices (a) 1-1, with $\tau = 1.6$; (b) 2-1, $\tau = 2.83$; (c) 3-1, $\tau = 4.08$; (d) 1-3, $\tau = 0.713$.

We note that we have only been able to successfully simulate the lowest-order modes for each container geometry investigated. This is not particularly surprising given the presence of viscosity and the fact the Reynolds numbers involved, while moderate, are not large. Fultz also only reported being able to successfully identify a similar number of the lowest indexed modes.

Resonance Conditions

In a flow with viscosity, as for Fultz's experiments and our simulations, one cannot expect sharp resonances as would occur in frictionless flow, although, since our Reynolds numbers are moderately large (the same, or of the same order, as for the experiments), reasonable indications should be observed. We are left with the question of how to assess resonance, since as noted above, Fultz's dye-visualisation methodology was rather subjective and also difficult to implement and assess in a numerical simulation. Instead we adopted two quantitative measures.

First, we compute the kinetic energy of the flow integrated over the simulation domain, either instantaneous or time-average. For a given paddle motion amplitude, it may be expected that the flow kinetic energy should be at a local maximum at a resonant frequency. We chose to compute the instantaneous kinetic energy for a fixed phase in the paddle motion cycle, once the flow had reached a periodic state. After some initial

investigation it was noted that the kinetic energy was dominated by the azimuthal (swirl) velocity component, which made the outcomes relatively insensitive to period ratio τ . Subsequently we computed kinetic energy based only on the radial and axial velocity components, corresponding approximately to a computation in the container frame of reference. We have normalised the kinetic energy with the square of the maximum paddle speed, here 4% of the maximum peripheral speed of the container.

Second, we examine the peak-to-peak magnitude of the force exerted by the paddle when the flow is time-periodic. Again we may expect that this would have a local minimum at a resonance, and again we have normalised the value by the square of the maximum paddle speed.

Outcomes are shown in Figure 6 and Figure 7 which are for $\delta = 0.5$ and 2.5 respectively. Note that in each figure, two curves are drawn, one (solid line) for simulations conducted with meshes designed to capture modes with an odd number of axial cells ($n = 1, 3$, etc.) and the other (dashed line) designed for modes with an even number of axial cells ($n = 2, 4$, etc.). Overall, there is a reasonable match between the inviscid predictions of resonant frequencies (eqn 3), and frequencies for maxima of kinetic energy, minima of paddle force magnitude obtained via our simulations.

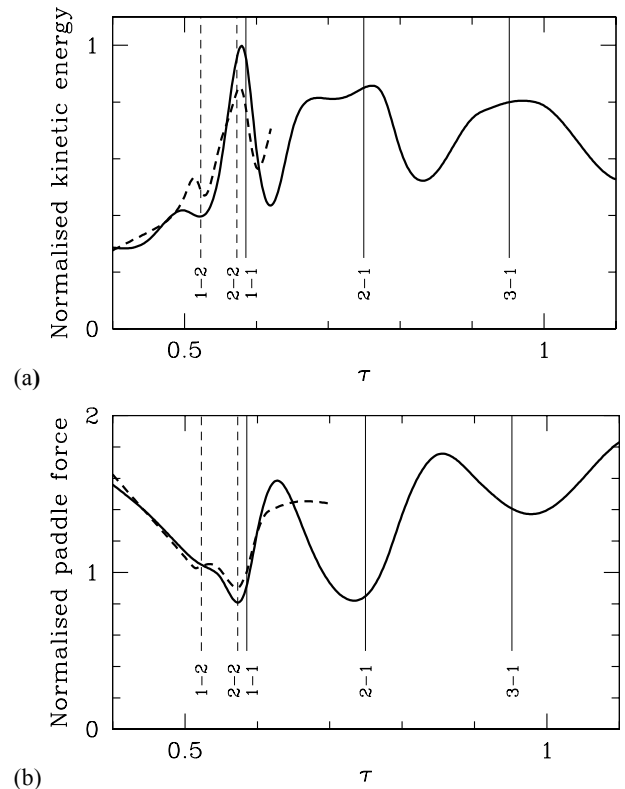


Figure 6. Normalised instantaneous flow kinetic energy (a) and normalised paddle force (b) as functions of period ratio (eqn 3) for container geometry $\delta = 0.5$. Solid curve, mesh designed for an odd number of axial cells (figure 3a); dashed curve, mesh designed for an even number of axial cells (figure 3b). Period ratios for various resonance conditions are indicated by vertical lines labelled with radial-axial cell indices.

The meshes designed to be used for modes with an even number of axial cells help reveal the lowest mode of this kind (the 1-2 mode). There do appear to be difficulties distinguishing the 1-1 mode and the 2-2 mode using these methods, which is unsurprising given the fact that the predicted frequencies for these modes are quite similar (see Figure 1). However, it is quite

straightforward to obtain a pure 1-1 mode shape in each geometry, as shown in *Figure 4* and *Figure 5*.

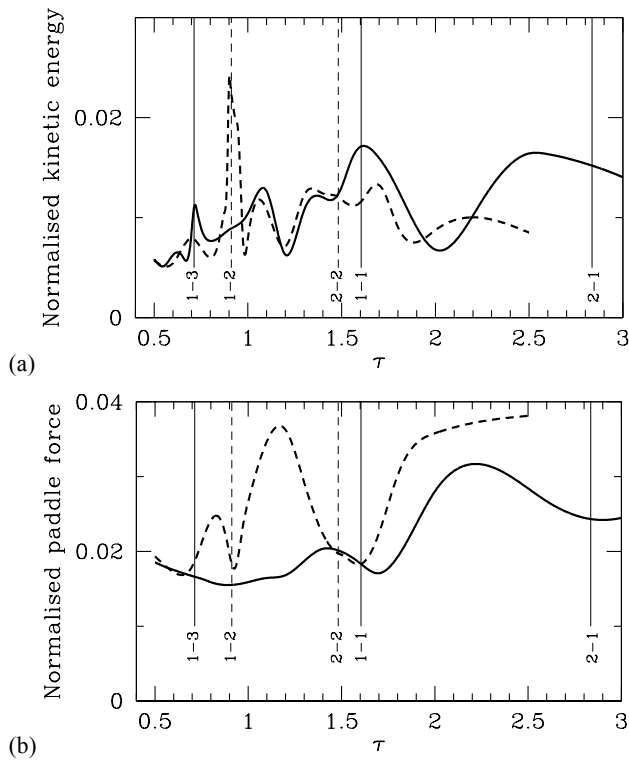


Figure 7. Normalised instantaneous flow kinetic energy (a) and normalised paddle force (b) as functions of period ratio (eqn 3) for container geometry $\delta = 2.5$. Solid curve, mesh designed for an odd number of axial cells; dashed curve, mesh designed for an even number of axial cells. Period ratios for various resonance conditions are indicated by vertical lines.

Conclusions

Our method for examining resonance conditions works quite well for predicting the lowest-order inertial wave resonances, and in fact agrees well with the experimental results obtained by Fultz. As might be expected, the simple quantitative measures of resonance are not particularly good for resolving modes that have very similar resonant frequencies, but otherwise perform adequately for isolated modes.

In future work on this problem we plan to carry out linear stability analysis of the flows for both axisymmetric and three-dimensional disturbances. However, we also intend to use these results to validate an extension to the DNS solver that will simulate flows in a general rotating reference frame (i.e. with centripetal and Coriolis terms explicitly represented) in addition to those described in an inertial reference frame.

References

- [1] Fultz D (1959). A note on overstability and the elastoid-inertia oscillations of Kelvin, Solberg, and Bjerknes. *Meteorology* **16** 199–208.
- [2] Greenspan, HP (1968). *Theory of Rotating Fluids*. Cambridge University Press.
- [3] Vanyo, JP (2001). *Rotating Fluids in Engineering and Science*. Dover.
- [4] Blackburn HM & Sherwin SJ (2004). Formulation of a Galerkin spectral element–Fourier method for three-dimensional incompressible flows in cylindrical geometries. *J Comput Phys* **197**, 759–778.